Reaction Chemistry & Engineering

ROYAL SOCIETY OF CHEMISTRY

PAPER

View Article Online
View Journal

Open Access Article. Published on 10 June 2025. Downloaded on 26/07/2025 9:01:36 PM.
This article is licensed under a Creative Commons Attribution 3.0 Unported Licence.

Check for updates

Cite this: DOI: 10.1039/d4re00181h

Efficacy of mechanochemically prepared ceria–zirconia catalysts in ketonisation of acetic acid†

Krutarth Pandit,[ab] Gunjan Deshmukh,[a] Dipti Wagh,[a] Vikram Chatake,[c] Aniruddha Pandit,[c] Supriyo Kumar Mondal,[b] Atul Bari,*[b] Nancy Artioli[ad] and Haresh Manyar*[a]

Received 4th April 2024,
Accepted 9th June 2025

DOI: 10.1039/d4re00181h

rsc.li/reaction-engineering

This work presents a comprehensive study on the catalytic and kinetic aspects of the ketonisation of acetic acid, a model volatile fatty acid, using $Ce_{1-x}Zr_xO_2$ as catalysts. Volatile fatty acids are promising biomass derived feedstock for production of drop-in sustainable aviation fuels through a series of cascade reactions, with ketonisation as the first step followed by aldol condensation and subsequent hydrogenation. A series of $Ce_{1-x}Zr_xO_2$ catalysts for ketonisation were prepared using a mechanochemical technique of ball milling, and their performance was evaluated for varying Ce/Zr mole ratios. Among the catalysts tested, $Ce_{0.75}Zr_{0.25}O_2$ exhibited the highest conversion and selectivity towards the desired product, acetone. The catalyst characterisation showed the formation of nano-aggregates with an average particle size of 340.8 nm and a specific surface area of 66.2 m^2 g^{-1}. The kinetics of the reaction indicated a second-order dependence on acetic acid, while the products (acetone, water, and CO_2) exhibited negative orders, suggesting competitive adsorption on the active sites of the catalyst. The activation energy for the reaction was determined to be 103.4 kJ mol^{-1} suggesting the surface reaction as the rate controlling step. These findings provide valuable insights into the catalytic behaviour and kinetics of the ketonisation reaction.

1. Introduction

The globally increasing demand for energy and dwindling crude oil reserves combined with the climate emergency have sparked rapid development of low carbon technologies to secure clean energy from renewable sources. Biomass has become a key focus as renewable feedstock for producing hydrogen, liquid transportation fuels, and platform chemicals.[1,2] Annually, the increase in greenhouse gas emissions continues to rise, causing difficulties in climate mitigation. A joint effort from all sectors is imperative to prevent dangerous climate crisis, and in this regard, the aviation industry holds a major contribution. The global consumption of aviation fuels, currently at 360 billion litres per year, is expected to double by 2050, posing to be a major challenge to the ambitious 2050 net zero target due to increasing greenhouse gas emissions. With the aviation industry committing to reduce its carbon footprint by 50% before 2050, increasing the production of sustainable aviation fuel (SAF) has taken centre stage. However, current SAF production is at less than 1% of global jet fuel demand. Hence, new chemical technologies using waste and renewable feedstocks are urgently needed to increase SAF production and meet the 2050 net zero target.[1,2]

Volatile fatty acids (VFAs), which are carboxylic acids ranging from C_2 to C_8, can be generated from wet waste sources such as food waste, animal manure, and wastewater sludge, making them potential feedstock for SAF.[3,4] Typically, anaerobic digestion of wet waste by microbial consortia produces CO_2 and CH_4, but this process can be modified to produce VFAs instead by arresting methanogenesis.[5–7] Biomass conversion pathways for aviation fuel, collectively referred to as "sustainable", require quantification of carbon intensity to ensure significant reductions compared to fossil fuel usage and to evaluate the benefits of each pathway comprehensively.[7]

In a recent life cycle analysis (LCA) of the investigated pathway, which involves VFA upgrading to SAF through sequential ketonisation and hydro-treating, researchers found that the process exhibits a carbon emission intensity below zero (−55 g CO_2 eq. MJ^{-1}). This is primarily due to the

[a] School of Chemistry and Chemical Engineering, Queen's University Belfast, David-Keir Building, Stranmillis Road, Belfast, BT9 5AG, UK. E-mail: h.manyar@qub.ac.uk
[b] Institute of Chemical Technology, Marathwada Campus, Jalna, Maharashtra, India. E-mail: ah.bari@marj.ictmumbai.edu.in
[c] Chemical Engineering Department, Institute of Chemical Technology, Mumbai, India
[d] Department of Civil, Environmental, Architectural Engineering and Mathematics, University of Brescia, Via Branze, 43, 25123 Brescia, Italy

† Electronic supplementary information (ESI) available. See DOI: https://doi.org/10.1039/d4re00181h

Open Access Article. Published on 10 June 2025. Downloaded on 26/07/2025 9:01:36 PM.
This article is licensed under a Creative Commons Attribution 3.0 Unported Licence.

avoidance of methane emissions that would otherwise occur if wet waste was landfilled.[8] Similar LCA studies on the upgrading of VFAs to diesel blendstocks and fatty acids to waxes and surfactants, have also demonstrated substantial reductions in carbon intensity when waste acids are valorised for fuel and chemical production.[9–11] Therefore, the upgrading of VFAs derived from wet waste for use as drop in blendstocks in SAF presents a promising pathway for decarbonisation.

The ketonisation reaction has gained recent attention due to its capability to upgrade bio-oil and its aqueous phase.[12–21] Ketonisation proves to be an effective technique for the upgrading of organic acids by converting them into ketones while simultaneously removing oxygen in the form of water and CO_2. This process results in an increase in the heating values of the bio-oil and a reduction in acidity. The produced ketones are valuable as they can serve as building blocks for further reactions such as C–C coupling and hydro-deoxygenation, enabling the production of hydrocarbons suitable for transportation fuels. By utilizing the ketonisation process, organic acids can be efficiently transformed into ketones, providing a promising pathway for the upgrading of bio-oil and the generation of high-quality hydrocarbon products for sustainable energy applications.[8,21–24] The reaction scheme for ketonisation of acetic acid is shown in Fig. 1.

Building on our ongoing research in environmental catalysis and low carbon clean energy technologies,[25–34] we have investigated the ketonisation of acetic acid using mechanochemically synthesised ceria–zirconia ($Ce_{1-x}Zr_xO_2$) mixed metal oxide catalysts as a model reaction. This transformation is highly relevant for upgrading VFAs into sustainable aviation fuels through a sequential process involving ketonisation, aldol condensation, and subsequent hydrogenation to produce C_8–C_{14} hydrocarbons. Mechanochemical synthesis offers distinct advantages over conventional hydrothermal methods for preparing ceria–zirconia mixed metal oxide catalysts. It reduces the number of synthesis steps and eliminates the need for solvents, making the process more sustainable and economically attractive, particularly for scale-up.[35,36] The solvent-free nature also aligns with green chemistry principles by minimising waste. Furthermore, the intense mechanical grinding promotes defect formation and reduces particle size, leading to higher surface area and enhanced lattice oxygen vacancies, both of which are critical for achieving high activity and selectivity in ketonisation reactions. Initially, efficacy of various compositions of $Ce_{1-x}Zr_xO_2$ catalysts is explored for establishing the optimal catalyst for ketonisation. Different catalyst compositions are prepared using the ball milling technique, followed by experimental investigations. The subsequent phase focuses on studying the kinetics of the reaction using the selected catalyst to determine the kinetic parameters. Both differential and integral reactor studies are conducted to gather the necessary kinetic data for fitting into a kinetic model. The kinetic modelling is performed using the Langmuir–Hinshelwood–Hougen–Watson (LHHW) mechanism, and a non-linear regression analysis is applied to determine the parameters based on the obtained experimental data. Through this approach, valuable insights into the catalytic ketonisation of acetic acid and the associated kinetic behaviour are obtained.

2. Experimental section

2.1 Materials

Acetic acid (>99%), acetone (99%), cerium oxide (CeO_2), and zirconium oxide (ZrO_2) were purchased from Molychem Chemicals, Mumbai, India. CO_2 and deionised water were also co-fed into the reactor. Nitrogen was used as a sweep gas. All other reagents were purchased from commercial sources and used as received, unless otherwise stated.

2.2 Experimental setup

The experimental setup comprises a phase change reactor designed to convert acetic acid from a liquid phase to a gas phase, facilitated by co-feeding of sweep gas nitrogen. Subsequently, the gaseous mixture is directed towards the catalyst bed within the main reactor for the conversion of acetic acid. After the conversion process, the gases undergo condensation in a condenser unit, where samples are extracted for analysis. The scheme for the experimental setup is shown in Fig. 2. The experimental setup used in this study involved the fixed-bed reactor configuration. Inside the main reactor, the catalyst is placed between quartz wool plugs, as shown in Fig. 3.

The flow rate of acetic acid was regulated using a peristaltic pump, with the system initially set at a stable flow rate for 60 minutes before taking subsequent samples. Furthermore, the gases CO_2 and N_2 were introduced into the system by co-feeding them through the gas cylinders *via* rotameters. The reactor temperature was controlled using a PID temperature controller. To collect the samples for

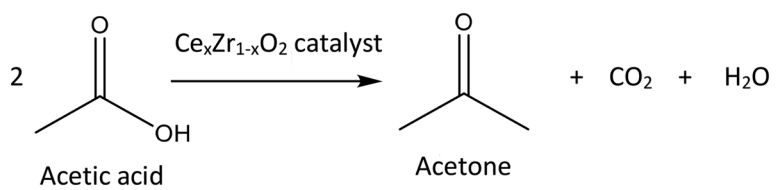

Fig. 1 Reaction scheme for ketonisation of acetic acid.

Open Access Article. Published on 10 June 2025. Downloaded on 26/07/2025 9:01:36 PM.
This article is licensed under a Creative Commons Attribution 3.0 Unported Licence.

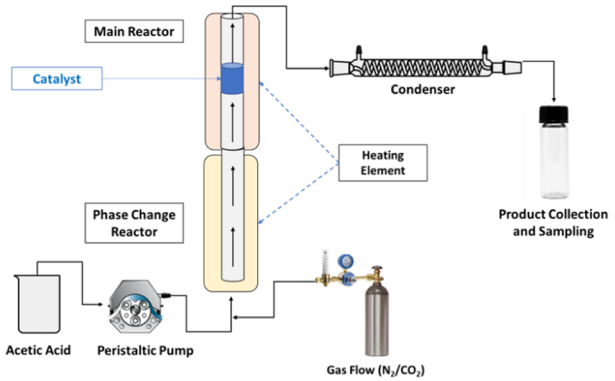

Fig. 2 Scheme for the experimental setup.

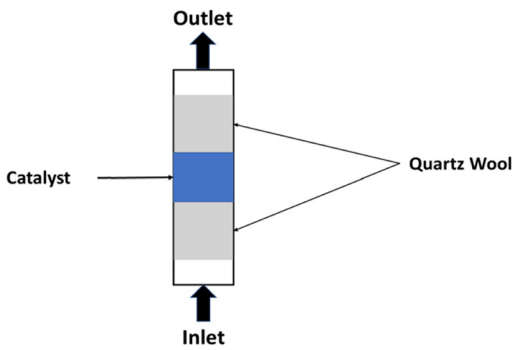

Fig. 3 Catalyst arrangement inside the reactor.

analysis, the feed exiting the reactor was condensed using cold water from a condenser.

2.3 Analysis of products

Analysis of acetic acid and acetone was carried out using a ThermoFisher UltiMate™ 3000 HPLC system equipped with a refractive index detector (ERC RefractoMax 520). The column selected for this analysis is the Hypersil GOLD™ C18 Selectivity HPLC Column (250 × 4.6 mm maximum pressure 400 bar and maximum temperature 60 °C) packed with spherical, fully porous, and ultrapure silica. The mobile phase consists of 0.005 M H_2SO_4, and a flow rate of 0.06 ml min^{-1} with a column temperature of 30 °C is maintained. The mobile phase and temperature were selected based on previous work by Kumar *et al.* for the analysis of acetic acid and acetone.[37] The calibration plots of acetic acid and acetone are shown in Fig. S1 of the ESI.†

The acetic acid conversion and selectivity towards acetone are estimated based on the concentrations obtained by HPLC. Equations are formulated by combining material balance and chemical reaction engineering principles, considering the reaction stoichiometry. Here, it is assumed that the products are formed in stoichiometric amount and the concentration of water and CO_2 in the system are calculated by material balance.

$$\text{Conversion } (X) = \frac{C_{\text{In}} - C_{\text{Out}}}{C_{\text{In}}} \quad (1)$$

C_{In} = inlet concentration of acetic acid (g mL^{-1})
C_{Out} = outlet concentration of acetic acid (g mL^{-1})

$$\text{Selectivity} = 2 \times \frac{\text{Moles of Acetone in Sample}}{\text{Moles of Acetic Acid Reacted}} = \frac{2n_{\text{Ketone}}}{n_{\text{acid,fed}}} \quad (2)$$

2.4 Catalyst preparation

The catalysts were prepared using commercially purchased cerium oxide (CeO_2) and zirconium oxide (ZrO_2) powders. A ball-milling method suggested by Puértolas *et al.* was used to prepare catalysts with varying Ce/Zr mole ratios at 150 rpm for 60 minutes.[38] The different catalysts prepared are listed below in Table 1.

3. Results and discussion

3.1 Effect of catalyst composition

This study evaluated the prepared catalysts with varying compositions for their performance in a fixed-bed reactor under similar reaction conditions. The reaction was carried out at a temperature of 350 °C with a catalyst loading of 2 g and a flow rate of 0.1 ml min^{-1}. Before initiating the reaction, the reactor was brought to a steady-state in terms of temperature and flow rate, which required around one hour. In this section, a solution of acetic acid with a weight-to-weight ratio of 50% was employed to investigate the effects of the aqueous stream on both the catalyst's stability and its subsequent yield. The results of this study are shown below in Fig. 4.

The results show the conversion and selectivity of acetic acid towards acetone for each of the catalysts tested. The conversion of the acetic acid varies in the order 75CeZr > 100Ce > 25CeZr > 100Zr > 50CeZr > 90CeZr > 10CeZr while the selectivity to acetone varies in the order 75CeZr > 100Ce > 50CeZr > 10CeZr > 90CeZr > 25CeZr > 100Zr.

We believe it can be attributed to the combination of the structural characteristics of the $Ce_{1-x}Zr_xO_2$ mixed oxide catalysts, which includes a fine balance between the surface acid–base sites, available surface area and dispersion of ZrO_2 nanoclusters on the surface of CeO_2. The results obtained from the study indicate that the 75CeZr catalyst exhibits the highest conversion and selectivity towards the target product,

Table 1 List of prepared catalysts

Ce/Zr (mole ratio)	Formula	Code
0 : 100	ZrO_2	100Zr
10 : 90	$Ce_{0.1}Zr_{0.9}O_2$	10CeZr
25 : 75	$Ce_{0.25}Zr_{0.75}O_2$	25CeZr
50 : 50	$Ce_{0.5}Zr_{0.5}O_2$	50CeZr
75 : 25	$Ce_{0.75}Zr_{0.25}O_2$	75CeZr
90 : 10	$Ce_{0.9}Zr_{0.1}O_2$	90CeZr
100 : 0	CeO_2	100Ce

Open Access Article. Published on 10 June 2025. Downloaded on 26/07/2025 9:01:36 PM.
This article is licensed under a Creative Commons Attribution 3.0 Unported Licence.

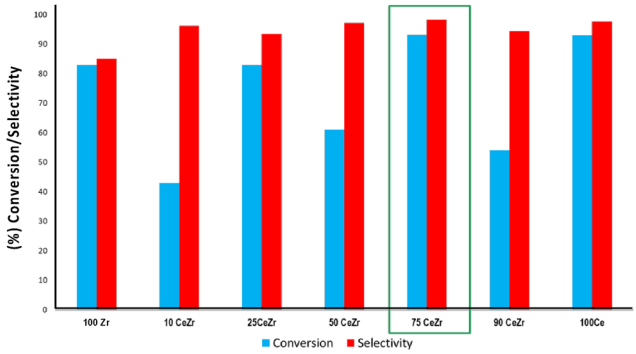

Fig. 4 Effects of catalyst composition. Reaction conditions: catalyst loading 2 g, reaction temperature 350 °C, and feed flow rate 0.1 ml min^{-1}.

thus making it the optimal catalyst for the target reaction. Thus, for studying kinetics, all further experiments were performed using 75CeZr as the catalyst.

3.2 Kinetic study

3.2.1 Differential reactor. The aim of this study was to determine the reaction order with respect to acetic acid and with respect to the products. It should be noted that at lower conversion, acetone, water, and CO_2 were the only products detected. Thus, we can assume that the converted acetic acid exhibited ≈100% selectivity towards the aforementioned products at lower conversion. Hence, the total conversion of acetic acid was maintained below 20% to ensure complete selectivity and prevent any unwanted side reactions. The ESI† shows that the obtained kinetic data were free from mass transfer limitations.

The rate of the reaction was calculated using eqn (3):

$$r = X \times \frac{F}{W} \tag{3}$$

where,

r = rate of the reaction (mol min^{-1} g_{cat}^{-1})

X = conversion

F = inlet molar flow rate (mol min^{-1})

W = catalyst weight (g)

To ascertain the reaction order with respect to acetic acid, the partial pressure of acetic acid was varied by modifying the inlet flow of the carrier gas (nitrogen). The total pressure was kept at a constant 760 mmHg with the total temperature at 300 °C. The acetic acid flow rate was kept at a constant value.

The impact of varying acetic acid partial pressures on the rate of the reaction is presented below in Fig. 5. As the conversion was low, it was assumed that the partial pressure of the products was insignificant compared to the partial pressure of acetic acid. Therefore, it is evident from Fig. 5 that the reaction order with respect to acetic acid is 1.675, which is consistent with previous findings reported in the literature.[20,39–41]

To further investigate the impact of product concentration on the reaction rate, varying quantities of acetone, water, and CO_2 were injected into the reactor, and the corresponding

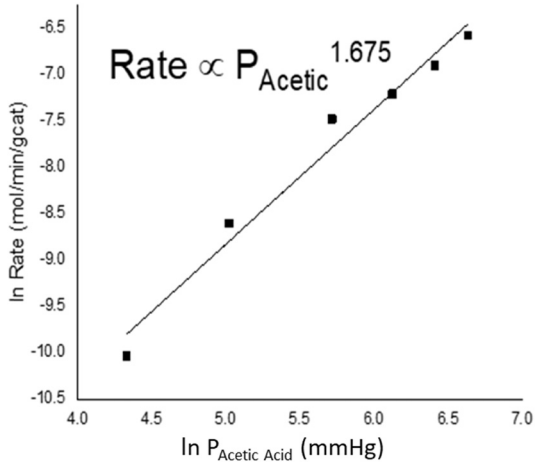

Fig. 5 Rate *vs.* partial pressure of acetic acid.

rates were measured. In the case of acetone and water, the feed proportions were adjusted to create different quantities of the mixture, which were then introduced into the reactor. To vary the CO_2 partial pressure, a calibrated cylinder of CO_2 was connected to the setup and CO_2 was fed into the reactor along with acetic acid.

The results indicate that all the products exerted an inhibitory effect on the reaction rate, with acetone demonstrating the most pronounced inhibition. On the other hand, the effect of water and CO_2 was significantly lower than that of acetone. The reaction orders with respect to acetone, water, and CO_2 were determined to be −0.418, −0.132, and −0.202, respectively. The findings are illustrated below in Fig. 6.

3.2.2 Integral reactor. In addition to conducting differential reactor studies, an integral reactor study was also conducted to explore the reaction, following the methodology outlined by Pham *et al.*[39,40] and Gaertner *et al.*[20] The integral reactor study was carried out at four different temperatures: 300 °C, 325 °C, 350 °C and 375 °C. To analyse the variation in partial pressure with changing residence time W/F (h), the residence time of the feed acetic acid was varied by adjusting the volumetric flow rate and calculating the corresponding residence time. The partial pressure was measured based on the conversion of acetic acid to acetone. The residence time has been determined by dividing the catalyst loading in grams (g) by the inlet mass flow rate of acetic acid in grams per hour (g h^{-1}). To verify if the calculated partial pressures were accurate, a material balance was performed based on the conversion of acetic acid.

The results at four different reaction temperatures are shown in Fig. 7. As expected, it is evident that as the residence time increases, the conversion of acetic acid also increases, leading to a decrease in the partial pressure of acetic acid and an increase in the partial pressure of acetone. The dotted lines represent the general trend of the graph.

3.3 Development of the kinetic model

From the differential reactor data, it can be inferred that the reaction follows a second-order kinetics with respect to acetic

Open Access Article. Published on 10 June 2025. Downloaded on 26/07/2025 9:01:36 PM.
This article is licensed under a Creative Commons Attribution 3.0 Unported Licence.

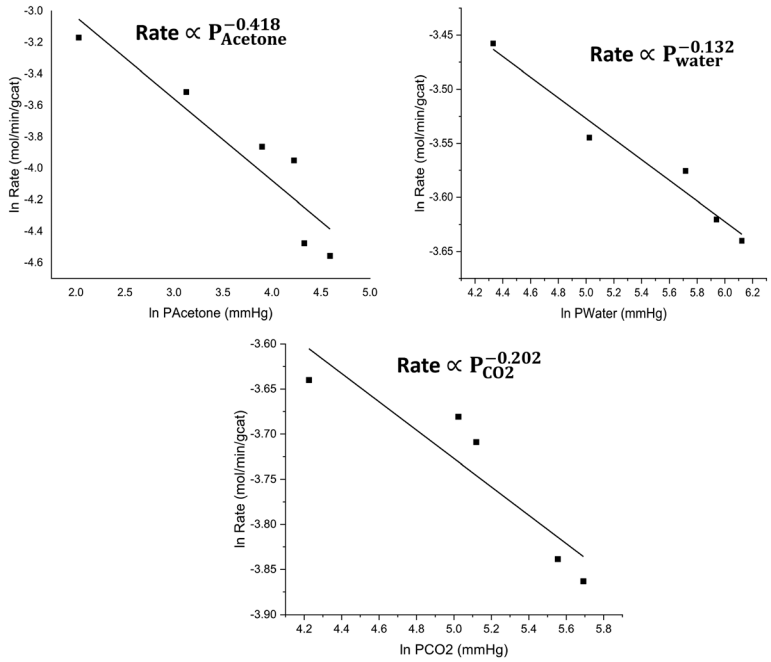

Fig. 6 Rates *vs.* partial pressures of acetone, water and carbon dioxide.

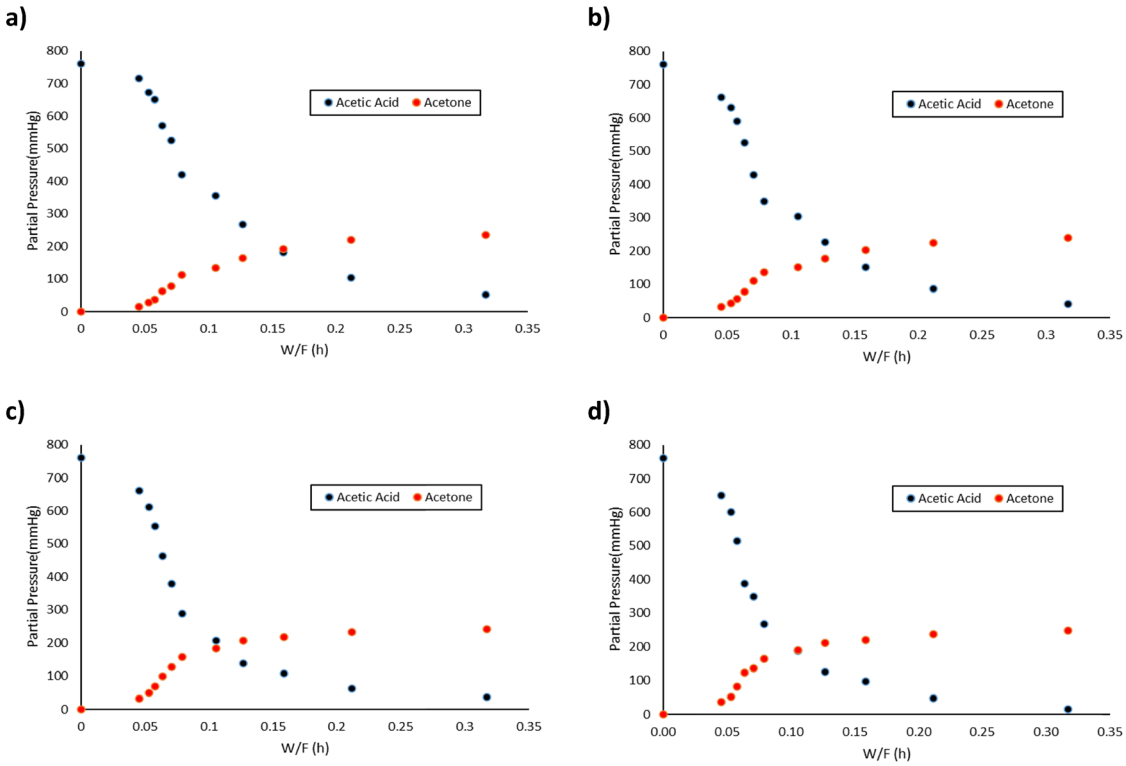

Fig. 7 Variation in partial pressures of acetone and acetic acid (mmHg) as a function of residence time (*W*/*F*) (h) on the 75CeZr catalyst (a: 300 °C, b: 325 °C, c: 350 °C, and d: 375 °C).

acid. Furthermore, the presence of reaction products hinders the reaction, indicating that there is a competition for the active sites on the catalyst. To account for these observations, a set of elementary reactions can be proposed and integrated into the LHHW kinetic model to effectively describe the reaction kinetics. This model incorporates a series of elementary reactions that describe the reaction kinetics, accounting for the competitive adsorption of reactant and product molecules on

Open Access Article. Published on 10 June 2025. Downloaded on 26/07/2025 9:01:36 PM.
This article is licensed under a Creative Commons Attribution 3.0 Unported Licence.

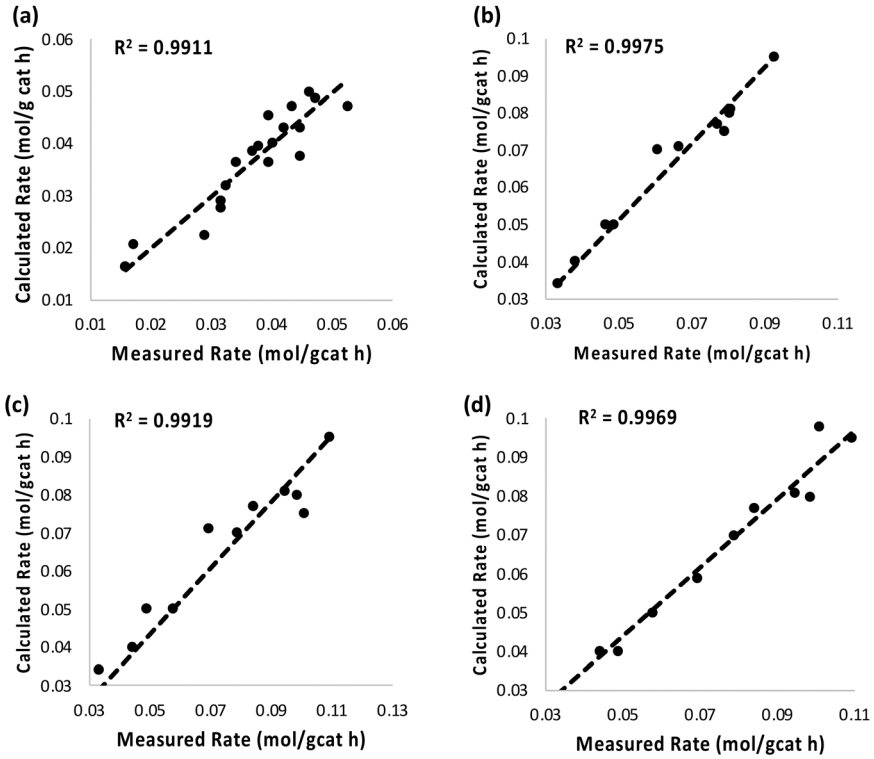

Fig. 8 Parity plots at (a) 300 °C, (b) 325 °C, (c) 350 °C and (d) 375 °C.

Table 2 Values of the rate and adsorption constants

Rate constant (k) mol g_{cat}^{-1} h^{-1}	K_{CH_3COOH} $mmHg^{-1}$	$K_{CH_3COCH_3}$	K_{H_2O}	K_{CO_2}	Temp. K
0.0636	0.0211 ± 0.079	0.0557 ± 0.02	0.0012 ± 0.01	0.0042 ± 0.001	573
0.1498	0.0193 ± 0.011	0.0342 ± 0.003	0.0062 ± 0.001	0.0042 ± 0.001	598
0.3312	0.0114 ± 0.0009	0.0211 ± 0.081	0.0050 ± 0.001	0.0040 ± 0.002	623
0.8168	0.0178 ± 0.013	0.0132 ± 0.0076	0.0037 ± 0.001	0.0038 ± 0.003	648

the catalyst surface. The proposed model is expected to provide valuable insights into the underlying reaction mechanisms and facilitate the optimisation of reaction conditions to improve reaction performance. The series of elementary reactions can be shown below based on the reaction behaviour observed in the differential reactor study and literature.[19,39,40]

$$CH_3COOH + * \overset{k_{acid}}{\leftrightarrow} CH_3COOH* \quad (4)$$

$$CH_3COCH_3 + * \overset{k_{ketone}}{\leftrightarrow} CH_3COCH_3* \quad (5)$$

$$CO_2 + * \overset{k_{CO_2}}{\leftrightarrow} CO_2* \quad (6)$$

$$H_2O + * \overset{k_{H_2O}}{\leftrightarrow} H_2O* \quad (7)$$

$$CH_3COOH* + CH_3COOH* \overset{k}{\rightarrow} CH_3COCH_3* + CO_2 + H_2O + * \quad (8)$$

Here, it should be noted that K_{acid}, K_{Ketone}, K_{CO_2}, and K_{H_2O} are the adsorption constants while the rate-determining step is eqn (8) where k is the kinetic factor. From the equations mentioned above, eqn (4)–(7) highlight the competitive adsorption of the reactants and products on the surface active sites of the catalysts as the same can be observed in the differential reactor expressions. Eqn (8) depicts the surface reaction considered to be the rate-determining step.

It is important to note that in the LHHW kinetic model for the reaction, the adsorption constants K_{acid}, K_{Ketone}, K_{CO_2}, and K_{H_2O} have been incorporated. The kinetic factor k for step 5 has been identified as the rate-determining step. Based on this rate-determining step, the overall rate of the reaction can be expressed using the appropriate mathematical expression.

$$\text{Rate} = k(\Theta_{CH_3COOH})^2 \quad (9)$$

In this context, the parameter Θ_{CH_3COOH} represents the fraction of active sites on the catalyst surface that are covered by acetic acid molecules. This value can be calculated using standard equations based on the adsorption equilibrium of the molecules.

Open Access Article. Published on 10 June 2025. Downloaded on 26/07/2025 9:01:36 PM.
This article is licensed under a Creative Commons Attribution 3.0 Unported Licence.

$$\Theta_{CH_3COOH} = K_{CH_3COOH}P_{CH_3COOH}\Theta_V \quad (10)$$

$$\Theta_{CH_3COCH_3} = K_{CH_3COCH_3}P_{CH_3COCH_3}\Theta_V \quad (11)$$

$$\Theta_{CO_2} = K_{CO_2}P_{CO_2}\Theta_V \quad (12)$$

$$\Theta_{H_2O} = K_{H_2O}P_{H_2O}\Theta_V \quad (13)$$

$$\Theta_{CH_3COOH} + \Theta_{CH_3COCH_3} + \Theta_{CO_2} + \Theta_{H_2O} + \Theta_V = 1 \quad (14)$$

Here, Θ_V represents the fraction of vacant sites, while Θ_{CH_3COOH}, $\Theta_{CH_3COCH_3}$, Θ_{CO_2}, and Θ_{H_2O} denote the fractional surface coverages of the respective species. Substituting these values of Θ_{CH_3COOH}, $\Theta_{CH_3COCH_3}$, Θ_{CO_2}, and Θ_{H_2O} into the above expression and factoring out Θ_V as a common term, the rate expression can be derived based on the conventional LHHW mechanism as follows:

$$\text{Rate} = k\frac{(K_{CH_3COOH}P_{CH_3COOH})^2}{(1 + K_{CH_3COOH}P_{CH_3COOH} + K_{CH_3COCH_3}P_{CH_3COCH_3} + K_{CO_2}P_{CO_2} + K_{H_2O}P_{H_2O})^2} \quad (8)$$

3.4 LHHW model fitting

To validate the developed kinetic model, a multi-variable non-linear regression model was developed in MATLAB®. The model was made based on the experimental data that was fed into the software. The input data utilised for the multi-variable non-linear regression model included both differential and integral reactor data obtained at 300 °C, as well as integral reactor data obtained at 325 °C, 350 °C, and 375 °C, respectively. Partial pressures ($P_{Acetic\ Acid}$, $P_{Acetone}$, P_{Water} and P_{CO_2}) along with the rate of reaction (r_A) were fed into the software. For this purpose, an lscurve fit (a solver for nonlinear least-squares problems) was utilised to estimate the unknown constants with the constraints of the given upper and lower bounds. The temperature dependence of the adsorption constants was modelled by using an Arrhenius type expression eqn (16) as shown below:

$$K_i = K_{i,0} \times e^{-\frac{\Delta H_{ads}}{RT}} \quad (16)$$

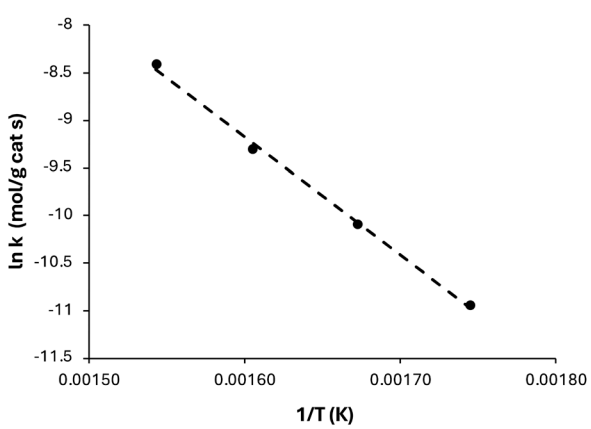

Fig. 9 ln k *vs.* 1/T.

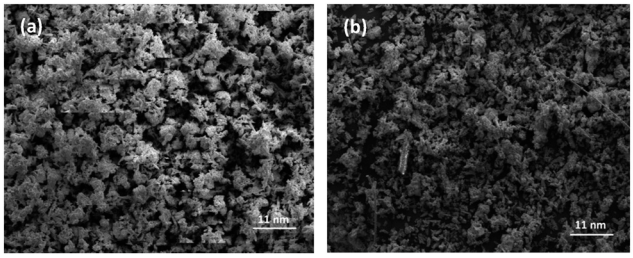

Fig. 10 SEM images of the (a) fresh catalyst and (b) spent catalyst.

Fig. 8 demonstrates that the calculated reaction rates by the model fit well with the actual measured reaction rates. Table 2 presents the results of the fitted data for the adsorption constants, including K_{CH_3COOH}, $K_{CH_3COCH_3}$, K_{CO_2}, and K_{H_2O}, and the rate constant k with their tolerance ranges.

Based on the rate constants obtained from nonlinear regression, we plotted ln k (mol g_{cat}^{-1} s^{-1}) *versus* 1/T (K), as shown in Fig. 9, in accordance with the Arrhenius equation. The apparent activation energy was estimated to be 103.4 kJ mol^{-1}, with an average frequency factor of 4.54 × 10^4. The value falls within the range reported in previous studies, such as Gaertner *et al.*,[20] who reported an activation energy of 57.7 kJ mol^{-1} for hexanoic acid ketonisation, and Pham *et al.*,[40] who predicted activation energies ranging from 156.4 to 220 kJ mol^{-1} for the ketonisation of acetic, propanoic and butyric acids. It is important to note that the range of activation energies observed signifies the variability in catalyst properties and their effectiveness in promoting the ketonisation reaction, as well as the variation in the reaction pathways. Also, the higher activation energy values indicate that the reaction is controlled by surface kinetics.

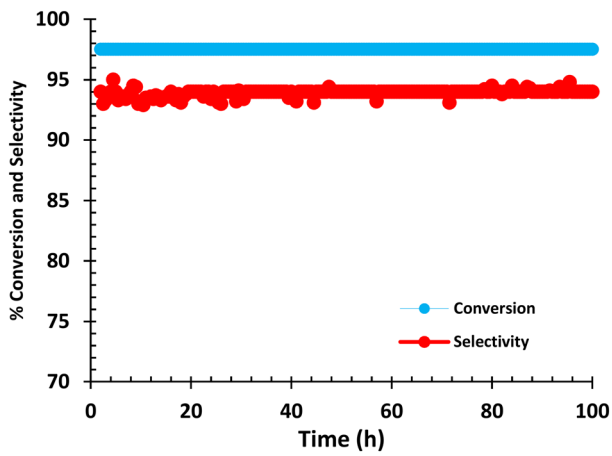

Fig. 11 Time on stream study. Reaction conditions: catalyst loading 2 g, reaction temperature 350 °C, and feed flow rate 0.1 ml min^{-1}.

Open Access Article. Published on 10 June 2025. Downloaded on 26/07/2025 9:01:36 PM. This article is licensed under a Creative Commons Attribution 3.0 Unported Licence.

3.5 Catalyst characterization

The catalyst's true and bulk densities were estimated using Archimedes' principle. The true density, representing the density of individual catalyst particles, was found to be 6500 kg m^{-3}, while the bulk density, which accounts for interparticle voids in the packed bed, was measured at 5314 kg m^{-3}. Brunauer–Emmett–Teller (BET) analysis using N_2 physisorption, Scanning Electron Microscopy (SEM) and particle size analysis were performed to estimate the necessary properties of the catalyst. The catalyst showed a BET surface area of 66 m^2 g^{-1}, with an average pore size of 19 nm. Dynamic Light Scattering (DLS) analysis indicated an average particle size of 340.8 nm. The elemental composition of all catalysts prepared was measured by inductively coupled plasma optical emission spectroscopy (ICP-OES) analysis using a Perkin-Elmer 4300. Additional catalyst characterisation studies of 75CeZr are provided in the ESI.†

The scanning electron microscope (SEM) images provide valuable insights into the particle morphology of the fresh and spent 75CeZr catalysts (Fig. 10). The images show no noticeable changes, indicating excellent morphological stability. This observation is further supported by the catalyst's stable performance under reaction conditions, as evidenced by the time-on-stream data in Fig. 11.

4. Conclusions and future scope

A comprehensive study of the ketonisation reaction was carried out using $Ce_{1-x}Zr_xO_2$ mixed metal oxide catalysts prepared *via* a mechanochemical ball milling approach. Among the catalysts tested, 75CeZr demonstrated the highest conversion and selectivity toward the desired product, acetone. The order of catalyst performance in terms of conversion was: 75CeZr > 100Ce > 25CeZr > 100Zr > 50CeZr > 90CeZr > 10CeZr, while selectivity followed: 75CeZr > 100Ce > 50CeZr > 10CeZr > 90CeZr > 25CeZr > 100Zr. Kinetic analysis indicated that the reaction follows a second-order rate law, with product inhibition observed due to competitive adsorption on active catalyst sites. The apparent activation energy of 103.4 kJ mol^{-1} further confirms the catalytic efficiency of the mechanochemically prepared materials.

Future studies will focus on evaluating catalyst performance with volatile fatty acids (VFAs) of higher chain lengths and assessing catalyst stability under conditions that closely mimic the complex composition of real VFA feedstocks such as hydrothermal liquefaction or anaerobic digestate aqueous phases. These studies will provide deeper insight into catalyst durability and activity in realistic applications.

Overall, the mechanochemically developed catalysts and the kinetic insights gained underscore the promising potential of this ketonisation process for upgrading waste streams from hydrothermal liquefaction.

Data availability

Data are available within the article and its ESI.†

Author contributions

K. P., G. D. and D. W.: methodology, investigation, and writing – original draft preparation. V. C. and S. K. M.: catalyst characterisation, analysis, and draft preparation. A. B., A. P., and N. A.: methodology and draft revision. H. M.: conceptualisation, visualisation, validation, writing – review & editing and resources.

Conflicts of interest

The authors declare that they have no known competing financial interests or personal relationships that could have appeared to influence the work reported in this paper.

Acknowledgements

The authors gratefully acknowledge the funding and support provided by the Leverhulme Trust research grant RPG-2020-301, as well as the UK Catalysis Hub *via* our membership of the UK Catalysis Hub Consortium funded by EPSRC grant: EP/R026645/1.

Notes and references

1 V. Thummala and R. B. Hiremath, Green aviation in India: Airline's implementation for achieving sustainability, *Clean. Responsible Consum.*, 2022, **7**, 100082, DOI: **10.1016/j.clrc.2022.100082**.

2 L. Zhang, T. L. Butler and B. Yang, Recent trends, opportunities and challenges of Sustainable aviation fuel, *Green Energy to Sustainability*, Wiley, 2020, pp. 85–110, DOI: **10.1002/9781119152057.ch5**.

3 A. H. Bhatt, Z. Ren and L. Tao, Value proposition of untapped wet wastes: carboxylic acid production through anaerobic digestion, *iScience*, 2020, **23**, 101221, DOI: **10.1016/j.isci.2020.101221**.

4 R. L. Skaggs, A. M. Coleman, T. E. Seiple and A. R. Milbrandt, Waste-to-Energy biofuel production potential for selected feedstocks in the conterminous United States, *Renewable Sustainable Energy Rev.*, 2018, **82**, 2640–2651, DOI: **10.1016/J.RSER.2017.09.107**.

5 G. R. Hafenstine, N. A. Huq, D. R. Conklin, M. R. Wiatrowski, X. Huo and Q. Guo, Single-phase catalysis for reductive etherification of diesel bioblendstocks, *Green Chem.*, 2020, **22**, 4463–4472, DOI: **10.1039/D0GC00939C**.

6 X. Huo, N. A. Huq, J. Stunkel, N. S. Cleveland, A. K. Starace and A. E. Settle, Tailoring diesel bioblendstock from integrated catalytic upgrading of carboxylic acids: a "fuel property first" approach, *Green Chem.*, 2019, **21**, 5813–5827, DOI: **10.1039/C9GC01820D**.

7 M. Atasoy, I. Owusu-Agyeman, E. Plaza and Z. Cetecioglu, Bio-based volatile fatty acid production and recovery from

 This journal is © The Royal Society of Chemistry 2025

Open Access Article. Published on 10 June 2025. Downloaded on 26/07/2025 9:01:36 PM.
This article is licensed under a Creative Commons Attribution 3.0 Unported Licence.

waste streams: Current status and future challenges, *Bioresour. Technol.*, 2018, **268**, 773–786, DOI: **10.1016/J.BIORTECH.2018.07.042**.

8 N. A. Huq, G. R. Hafenstine, X. Huo, H. Nguyen, S. M. Tifft and D. R. Conklin, Toward net-zero sustainable aviation fuel with wet waste–derived volatile fatty acids, *Proc. Natl. Acad. Sci. U. S. A.*, 2021, **118**(13), e2023008118, DOI: **10.1073/pnas.2023008118**.

9 N. A. Huq, X. Huo, G. R. Hafenstine, S. M. Tifft, J. Stunkel and E. D. Christensen, Performance-advantaged ether diesel bioblendstock production by a priori design, *Proc. Natl. Acad. Sci. U. S. A.*, 2019, **116**, 26421–26430, DOI: **10.1073/pnas.1911107116**.

10 B. Boekaerts, M. Vandeputte, K. Navaré, J. Van Aelst, K. Van Acker and J. Cocquyt, Assessment of the environmental sustainability of solvent-less fatty acid ketonization to bio-based ketones for wax emulsion applications, *Green Chem.*, 2021, **23**, 7137–7161, DOI: **10.1039/D1GC02430B**.

11 D. Schowanek, T. Borsboom-Patel, A. Bouvy, J. Colling, J. A. de Ferrer and D. Eggers, New and updated life cycle inventories for surfactants used in European detergents: summary of the ERASM surfactant life cycle and ecofootprinting project, *Int. J. Life Cycle Assess.*, 2018, **23**, 867–886, DOI: **10.1007/S11367-017-1384-X/TABLES/6**.

12 D. Alonso, J. Bond, J. Serrano-Ruiz and J. A. Dumesic, Production of liquid hydrocarbon transportation fuels by oligomerization of biomass-derived C9 alkenes, *Green Chem.*, 2010, **12**, 992–999, DOI: **10.1039/C001899F**.

13 J. Serrano-Ruiz, D. Wang and J. A. Dumesic, Catalytic upgrading of levulinic acid to 5-nonanone, *Green Chem.*, 2010, **12**, 574–577, DOI: **10.1039/B923907C**.

14 E. L. Kunkes, D. A. Simonetti, R. M. West, J. C. Serrano-Ruiz, C. A. Gärtner and J. A. Dumesic, Catalytic conversion of biomass to monofunctional hydrocarbons and targeted liquid-fuel classes, *Science*, 2008, **322**, 417–421, DOI: **10.1126/SCIENCE.1159210**.

15 S. H. Hakim, B. H. Shanks and J. A. Dumesic, Catalytic upgrading of the light fraction of a simulated bio-oil over CeZrOx catalyst, *Appl. Catal., B*, 2013, **142–143**, 368–376, DOI: **10.1016/j.apcatb.2013.05.021**.

16 M. A. Jackson, Ketonization of model pyrolysis bio-oil solutions in a plug-flow reactor over a mixed oxide of Fe, Ce, and Al, *Energy Fuels*, 2013, **27**(7), 3936–3943, DOI: **10.1021/ef400789z**.

17 R. W. Snell and B. H. Shanks, Ceria calcination temperature influence on acetic acid ketonization: mechanistic insights, *Appl. Catal., A*, 2013, **451**, 86–93, DOI: **10.1016/j.apcata.2012.08.043**.

18 R. W. Snell and B. H. Shanks, Insights into the ceria-catalyzed ketonization reaction for biofuels applications, *ACS Catal.*, 2013, **3**(4), 783–789, DOI: **10.1021/cs400003n**.

19 C. Gaertner, J. Serrano-Ruiz, D. J. Braden and J. A. Dumesic, Catalytic coupling of carboxylic acids by ketonization as a processing step in biomass conversion, *J. Catal.*, 2009, **266**(1), 71–78, DOI: **10.1016/j.jcat.2009.05.015**.

20 C. A. Gaertner, J. C. Serrano-Ruiz, D. J. Braden and J. A. Dumesic, Ketonization reactions of carboxylic acids and esters over ceria–zirconia as biomass-upgrading processes, *Ind. Eng. Chem. Res.*, 2010, **49**, 6027–6033, DOI: **10.1021/IE1004338**.

21 F. Lin, W. Hu, N. R. Jaegers, F. Gao, J. Z. Hu, H. Wang and Y. Wang, Elucidation of the Roles of Water on the Reactivity of Surface Intermediates in Carboxylic Acid Ketonization on TiO2, *J. Am. Chem. Soc.*, 2023, **145**(1), 99–109, DOI: **10.1021/jacs.2c08511**.

22 J. A. Hayward, D. A. O'Connell, R. J. Raison, A. C. Warden, M. H. O'Connor and H. T. Murphy, The economics of producing sustainable aviation fuel: a regional case study in Queensland, Australia, *GCB Bioenergy*, 2015, **7**, 497–511, DOI: **10.1111/gcbb.12159**.

23 J. H. Miller, G. R. Hafenstine, H. H. Nguyen and D. R. Vardon, Kinetics and Reactor Design Principles of Volatile Fatty Acid Ketonization for Sustainable Aviation Fuel Production, *Ind. Eng. Chem. Res.*, 2022, **61**, 2997–3010, DOI: **10.1021/acs.iecr.1c04548**.

24 D. R. Vardon, B. J. Sherbacow, K. Guan, J. S. Heyne and Z. Abdullah, Realizing "net-zero-carbon" sustainable aviation fuel, *Joule*, 2022, **6**, 16–21, DOI: **10.1016/j.joule.2021.12.013**.

25 M. Delarmelina, G. Deshmukh, A. Goguet, R. Catlow and H. Manyar, Role of Sulfation of Zirconia Catalysts in Vapor Phase Ketonization of Acetic Acid, *J. Phys. Chem. C*, 2021, **125**(50), 27578–27595, DOI: **10.1021/acs.jpcc.1c06920**.

26 J. Ethiraj, D. Wagh and H. Manyar, Advances in Upgrading Biomass to Biofuels and Oxygenated Fuel Additives Using Metal Oxide Catalysts, *Energy Fuels*, 2022, **36**(3), 1189–1204, DOI: **10.1021/acs.energyfuels.1c03346**.

27 J. Keogh, C. Jeffrey, M. S. Tiwari and H. Manyar, Kinetic Analysis of Glycerol Esterification Using Tin Exchanged Tungstophosphoric Acid on K-10, *Ind. Eng. Chem. Res.*, 2023, **62**(45), 19095–19103, DOI: **10.1021/acs.iecr.2c01930**.

28 K. Pandit, C. Jeffrey, J. Keogh, M. S. Tiwari, N. Artioli and H. Manyar, Techno-Economic Assessment and Sensitivity Analysis of Glycerol Valorization to Biofuel Additives via Esterification, *Ind. Eng. Chem. Res.*, 2023, **62**(23), 9201–9210, DOI: **10.1021/acs.iecr.3c00964**.

29 M. S. Tiwari, D. Wagh, J. S. Dicks, J. Keogh, M. Ansaldi, V. V. Ranade and H. Manyar, Solvent Free Upgrading of 5-Hydroxymethylfurfural (HMF) with Levulinic Acid to HMF Levulinate Using Tin Exchanged Tungstophosphoric Acid Supported on K-10 Catalyst, *ACS Org. Inorg. Au*, 2023, **3**(1), 27–34, DOI: **10.1021/acsorginorgau.2c00027**.

30 G. D. Yadav and H. Manyar, Synthesis of a Novel Redox Material UDCaT-3: An Efficient and Versatile Catalyst for Selective Oxidation, Hydroxylation and Hydrogenation Reactions, *Adv. Synth. Catal.*, 2008, **350**(14–15), 2286–2294, DOI: **10.1002/adsc.200800313**.

31 N. Skillen, K. Ralphs, D. Craig, S. McCalmont, A. F. V. Muzio, C. O'Rourke, H. Manyar and P. K. J. Robertson, Photocatalytic reforming of glycerol to H2 in a thin film Pt-TiO2 recirculating photoreactor, *J. Chem. Technol. Biotechnol.*, 2020, **95**(10), 2619–2627, DOI: **10.1002/jctb.6444**.

Open Access Article. Published on 10 June 2025. Downloaded on 26/07/2025 9:01:36 PM.
This article is licensed under a Creative Commons Attribution 3.0 Unported Licence.

32 T. Jakubek, K. Ralphs, A. Kotarba and H. Manyar, Nanostructured potassium-manganese oxides decorated with Pd nanoparticles as efficient catalysts for low-temperature soot oxidation, *Catal. Lett.*, 2019, **149**, 100–106, DOI: **10.1007/s10562-018-2585-z**.

33 M. T. Yilleng, E. C. Gimba, G. I. Ndukwe, I. M. Bugaje, D. W. Rooney and H. Manyar, Batch to continuous photocatalytic degradation of phenol using TiO2 and Au-Pd nanoparticles supported on TiO2, *J. Environ. Chem. Eng.*, 2018, **6**, 6382–6389, DOI: **10.1016/j.jece.2018.09.048**.

34 R. O'Donnell, K. Ralphs, M. Grolleau, H. Manyar and N. Artioli, Doping Manganese Oxides with Ceria and Ceria Zirconia Using a One-Pot Sol–Gel Method for Low Temperature Diesel Oxidation Catalysts, *Top. Catal.*, 2020, **63**, 351–362, DOI: **10.1007/s11244-020-01250-x**.

35 J. Keogh, G. Deshmukh and H. Manyar, Green synthesis of glycerol carbonate via transesterification of glycerol using mechanochemically prepared sodium aluminate catalysts, *Fuel*, 2022, **310**, 122484, DOI: **10.1016/j.fuel.2021.122484**.

36 K. Ralphs, G. Collins, H. Manyar, S. L. James and C. Hardacre, Selective Hydrogenation of Stearic Acid Using Mechanochemically Prepared Titania-Supported Pt and Pt–Re Bimetallic Catalysts, *ACS Sustainable Chem. Eng.*, 2022, **10**(21), 6934–6941, DOI: **10.1021/acssuschemeng.1c07595**.

37 M. Kumar, S. Saini and K. Gayen, Acetone-butanol-ethanol fermentation analysis using only high performance liquid chromatography, *Anal. Methods*, 2014, **6**, 774–781, DOI: **10.1039/C3AY41717D**.

38 B. Puértolas, T. C. Keller, S. Mitchell and J. Pérez-Ramírez, Deoxygenation of bio-oil over solid base catalysts: From model to realistic feeds, *Appl. Catal., B*, 2016, **184**, 77–86, DOI: **10.1016/j.apcatb.2015.11.017**.

39 T. N. Pham, D. Shi and D. E. Resasco, Reaction kinetics and mechanism of ketonization of aliphatic carboxylic acids with different carbon chain lengths over Ru/TiO2 catalyst, *J. Catal.*, 2014, **314**, 149–158, DOI: **10.1016/J.JCAT.2014.04.008**.

40 T. N. Pham, D. Shi, T. Sooknoi and D. E. Resasco, Aqueous-phase ketonization of acetic acid over Ru/TiO2/carbon catalysts, *J. Catal.*, 2012, **295**, 169–178, DOI: **10.1016/j.jcat.2012.08.012**.

41 C. A. Gaertner, J. C. Serrano-Ruiz, D. J. Braden and J. A. Dumesic, Catalytic coupling of carboxylic acids by ketonization as a processing step in biomass conversion, *J. Catal.*, 2009, **266**, 71–78, DOI: **10.1016/j.jcat.2009.05.015**.

 This journal is © The Royal Society of Chemistry 2025